Energy & Environmental Science

Accepted Manuscript

This is an *Accepted Manuscript*, which has been through the Royal Society of Chemistry peer review process and has been accepted for publication.

Accepted Manuscripts are published online shortly after acceptance, before technical editing, formatting and proof reading. Using this free service, authors can make their results available to the community, in citable form, before we publish the edited article. We will replace this *Accepted Manuscript* with the edited and formatted *Advance Article* as soon as it is available.

You can find more information about *Accepted Manuscripts* in the Information for Authors.

Please note that technical editing may introduce minor changes to the text and/or graphics, which may alter content. The journal's standard Terms & Conditions and the Ethical guidelines still apply. In no event shall the Royal Society of Chemistry be held responsible for any errors or omissions in this *Accepted Manuscript* or any consequences arising from the use of any information it contains.

ROYAL SOCIETY OF CHEMISTRY

www.rsc.org/ees

Energy & Environmental Science

RSCPublishing

COMMUNICATION

SnO_2 Nanocrystals-decorated Mesoporous ZSM-5 as Precious Metal-free Electrode Catalyst for Methanol Oxidations

Cite this: DOI: 10.1039/xoxxoooooox

Received ooth January 2012,
Accepted ooth January 2012

DOI: 10.1039/xoxxoooooox

www.rsc.org/

Xiangzhi Cui, Yan Zhu, Zile Hua, Jingwei Feng, Ziwei Liu, Lisong Chen and Jianlin Shi*

A novel precious metal-free electrode catalyst SnO_2/m-ZSM-5 nanocomposite has been successfully synthesized. This SnO_2/m-ZSM-5 nanocomposite shows high and stable electrochemical catalytic activity for methanol oxidations, which is comparable to the Pt/C. The high electrochemical performance has been attributed to the synergetic catalytic effects between mesoporous ZSM-5 matrix and loaded SnO_2 nanocrystals.

Comparing with proton exchange membrane fuel cells (PEMFCs) using hydrogen as the fuel, direct methanol fuel cells (DMFCs) possess a number of advantages such as compatibility with the existing petroleum distribution network due to the consumption of liquid fuel, and feasibility to handle water and heat management.[1-5] However, the overall energy efficiency of DMFCs is much lower than that of their H_2-PEM counterparts mainly because of the high over potential necessary to oxidize methanol at the anode of DMFCs,[6, 7] and the related to this problem is the issue of anode electro-catalyst CO poisoning of the precious metal catalyst such as Pt. In addition, methanol oxidation is a catalyst-driven process and the products formed are HCHO, HCOOH, and CO_2 along with some other intermediates. [8, 9]

Hitherto, platinum (Pt) has still been the primary choice for catalyzing methanol oxidation.[10] However, several inherent drawbacks such as limited reserve, high cost, susceptibility to time-dependent drift and poor CO tolerance, have, to a large extent, prevented the DMFC from industrialization.[11] In order to overcome the sluggish kinetics and catalyst surface poisoning of Pt, great efforts and progresses have been made. One significant strategy to reduce Pt usage as well as enhance its catalytic activity and stability is to incorporate other precious or transition metals into it to form alloys, such as binary (PtRu, [12,13] Pt-Pd, [14-17] Pt-Rh,[18-20] Rh-Ni, [21] Pt-Au,[22] Pt-Ag, [23] Pt-Cu,[24,25] Pt-Ni,[26] Pt-Co,[27] Pt-Mo [28]), ternary (Pt-Pd-Co,[29] Pt-Ru-Co,[30] Pt-Ru-Fe [31]) and even quaternary (Pt-Ru-Ir-Os, [32] Pt-Ru-Mo-W, [33] Pt-Ru-Rh-Ni,[34] Pt-Ru-Ni-Zr [35]) or core-shell architectures. [29, 36] In spite of the enhanced mass activity and CO tolerance of the Pt-based catalyst, the cost of electrode catalyst is still unacceptable because of the use of other precious metals such as Ru, Rh, Pd, Au and Ag. On the other hand, the poor stability issue of the ternary or quaternary catalyst systems still needs to be improved substantially. Thus, searching for novel low-cost anode catalyst for methanol oxidation with high electrochemical catalytic activity and CO tolerance is still a great challenge for the wide applications of the DMFCs.

Aluminosilicate zeolites with hierarchical pore structures, in particular those containing nanosized mesoporosity interconnected with microporosity, have attracted extensive research attention because of their potential applications in catalyzing bulky reactants, as well as their mesoporosity-derived multi-functionalization availability.[37-39] Zeolites themselves serve as active and selective solid-acid catalysts in the petrochemical industry, but they are also widely used as supports to prepare bi-functional catalysts for catalyzing hydrocracking, hydro-isomerization and hydrocarbon aromatization processes, and etc.[40–42] However, the electrochemical catalytic performance of zeolite or zeolite-based materials, especially the electro-catalytic activity for methanol oxidation, has not been reported as far as we know.

Herein, we report a novel nanocomposite for methanol oxidation with tin dioxide nanocrystals (~3 nm) being homogeneously decorated on the surface of mesoporous zeolite (m-ZSM-5) spheroidicities, as a precious metal-free anode catalyst in DMFCs. SnO_2 with special electrochemical property has been used widely in lithium ion batteries (LIB) and even been reported to potentially replace commercial graphite as the LIB anode.[43-46] It is found in this report that SnO_2 loaded mesoporous ZSM-5 (SnO_2/m-ZSM-5) nanocomposite catalyst shows high and stable electrochemical catalytic activity for methanol oxidation, and the catalytic activity is comparable with the commercial Pt/C catalyst. SnO_2 crystals were dispersed homogeneously on the surface of mesoporous zeolite particles by using electrostatic interaction method as shown in Scheme 1. In step I, mesoporous ZSM-5 spheroidicities (about 300–400 nm in diameter) are firstly synthesized by a hydrothermal method, then its surface was modified by using organosilane TPHAC (octadecyldimethyl (3-trimethoxysilyl propyl) ammonium chloride) as active agent to make the mesoporous ZSM-5 surface positively charged, and the alkaline $SnO_2(OH)^-$ species were then easily adsorbed homogeneously on the zeolite surface by electrostatic effect as shown in step II. After heat treatment (step III), the organosilane was removed and SnO_2 nanocrystals was decorated homogeneously on the outer/inner surface of mesoporous ZSM-5

Energy & Environmental Science Accepted Manuscript

spheroidicity. As meso-ZSM-5 possess both outer surface and inner mesopore surface, SnO_2 nanocrystals are believed to be dispersed on both surfaces. The detailed structure schematics of SnO_2 nanoparticle distribution on the out/inner surfaces of a mesoporous ZSM-5 particle can be seen in Scheme S1†.

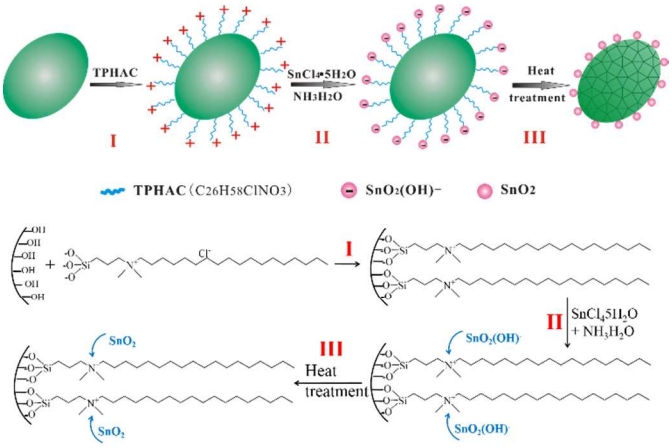

Scheme 1. Schematic design and synthesis of SnO_2 nanocrystal-decorated mesoporous ZSM-5 spheroidicity (SnO_2/m-ZSM-5). Step I, mesoporous ZSM-5 spheroidicity surface is modified by organosilane TPHAC to form a positive charge layer; Step II, alkaline $SnO_2(OH)^-$ species being adsorbed homogeneously on the zeolite surface by electrostatic attraction; Step III, after heat treatment, organosilane was removed and SnO_2 crystals were decorated homogeneously on the inner/outer surfaces of mesoporous ZSM-5 spheroidicity.

The synthesized SnO_2/m-ZSM-5 composite shows the characteristic peaks of ZSM-5 (Figure S1†) though with relatively low peak intensity. The morphology and microstructure of the as-derived SnO_2/m-ZSM-5 nanocomposites were characterized by field-emission scanning electron microscopy (FESEM) and transmission electron microscopy (TEM). It can be clearly seen from the FESEM images (Figure. 1A and B) that the morphology of mesoporous ZSM-5 is axiolitic with a diameter of about 350 nm. After the SnO_2 nanocrystal decoration, the morphology of the SnO_2/m-ZSM-5 nanocomposite remains unchanged from the SEM (Figure 1C and D) and the TEM (up-right inset in Figure 1E) images, moreover, mesoporous pores can still be seen clearly according to the magnified SEM images (Figure S2†). Furthermore, SnO_2 nanocrystals were dispersed homogeneously on/in the mesoporous ZSM-5 spheroidicity according to the elemental mappings (Figure 1D1, D2 and D3), in which no apparent aggregation can be found. EDX spectrum (Figure 1E) and high resolution TEM image (HRTEM, Figure 1F) consolidate the successful decoration of SnO_2 nanocrystals on/in m-ZSM-5 with a loading amount of 3.8 wt % (see data in Table S1†), and the measured lattice d-spacing of 0.32 nm agrees well with the SnO_2 (110) lattice plane of d = 0.3362 nm (JCPDS 46-1088). The particle size of SnO_2 crystal is about 3 nm estimated from the HRTEM image (down-right inset in Figure 1F), further indicating the successful dispersion of SnO_2 nanocrystals on/in mesoporous ZSM-5 by the surface electrostatic interaction method. It can also be calculated from the nitrogen sorption isotherms (Figure S3†) that the BET surface area of SnO_2/m-ZSM-5 nanocomposite is 371 m^2 g^{-1}, a little lower than that of m-ZSM-5 (see data in Table S1†) because of the loading of SnO_2 nanocrystals. Moreover, SnO_2/m-ZSM-5 nanocomposite exhibits hierarchically porous structure (Figure S2† and S3B†), different from those of SnO_2 supported mesoporous silica (such as SnO_2/SBA-15 and SnO_2/KIT-6 in Figure S4†), ɤ-Al_2O_3 (SnO_2/ ɤ-Al_2O_3 in Figure S4†), or even zeolite (SnO_2/ZSM-5, Figure. S6†), which would be favorable for the high electrochemical catalytic property of SnO_2/m-ZSM-5 nanocomposite as described below.

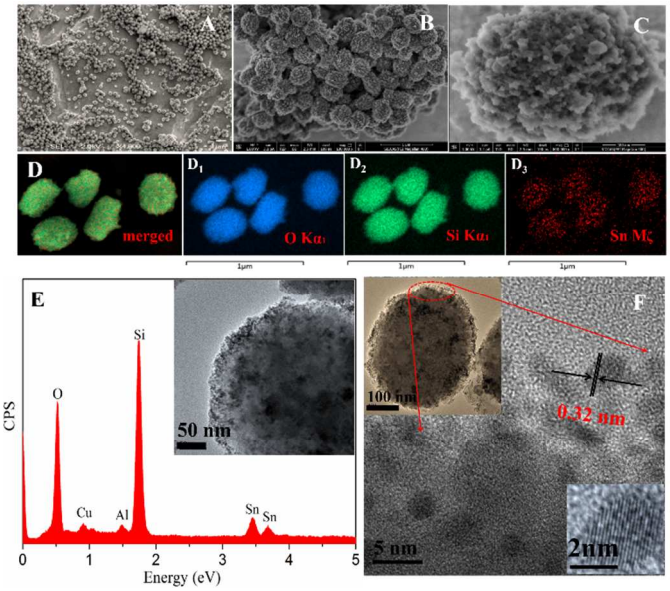

Figure. 1 SEM images of mesoporous ZSM-5 (A, B), SnO_2/m-ZSM-5 (C, D) and the element mappings (D1~D3) of image (D); TEM images of SnO_2/m-ZSM-5 (the up-right inset in E and the up-left in F) and the corresponding EDX spectrum (E); (F) high resolution TEM (HRTEM) of SnO_2/m-ZSM-5 of the circled area in the up-left inset in (F), and the down-right inset is the HRTEM image of a SnO_2 nanocrystal.

Figure 2 gives the typical cyclic voltammetry (CV) curves of the prepared samples in 0.5 M NaOH aqueous electrolyte. SnO_2/m-ZSM-5 shows a current density of 8.5 A g^{-1} (mass activity), which is comparable to that (9 A g^{-1}) of the commercial catalyst 20 wt %Pt/C-JM (Johnson Matthey). For comparison, the electrochemical activity of SnO_2 nano-powder prepared by sol-gel method (see SEM images in Figure.S5†) was also tested as shown in Figure.2A. It can be found that both pure m-ZSM-5 and pure SnO_2 nano-powder show much lower electrochemical catalytic activities. In addition, no clear current peak of carbon (XC-72R) could be identified, indicating that the carbon black only plays a role of electron-conducting support during the electrochemical test of SnO_2@m-ZSM-5. Thus, the high electrochemical catalytic activity of SnO_2/m-ZSM-5 nanocomposite should be due to the cooperative effects between SnO_2 nanocrystals and mesoporous ZSM-5 matrix. It also can be found from Figure 2B that the electrochemical activity of SnO_2/m-ZSM-5 nanocomposite increases with the increasing scan rate, suggesting a diffusion controlled process within the range of scan rates.[47] Two pairs of current peaks can be observed at the scan rate below 0.02 V s^{-1}, one at -0.84 *vs* -0.88 V for H-desorption and H^+-reduction, the other at -0.78 *vs* -0.82 V for H-oxidation and H^+-reduction, which are similar with those of Pt/C (Figure 2A). No significant decrease in peak current density for hydrogen oxidation can be detected for SnO_2/m-ZSM-5 nanocomposite after cycled for 100 times as shown in the inset of Figure. 2C, and the current density still keeps at above 90% even cycled for 1000 times (Figure 2C), indicating the stable electrochemical activity of the SnO_2/m-ZSM-5 spheroidicities. In contrast, SnO_2/ZSM-5, SnO_2/SBA-15, SnO_2/KIT-6 and SnO_2/ɤ-Al_2O_3 nanocomposites synthesized by the same procedure as SnO_2/m-ZSM show much lower current densities (Figure S10†), though with equally well dispersed SnO_2 nanocrystals at the same

Energy & Environmental Science Accepted Manuscript

This journal is © The Royal Society of Chemistry 2012

SnO_2 loading amount (see Figure. S6†, S7†, S8† and S9†, and the data in Table S1†).

For Pt/C catalyst, the electrochemical catalytic reaction in alkaline electrolyte should be:

$$H \leftrightarrow H^+ + e^- \quad (1)$$

$$H^+ + OH^- \leftrightarrow H_2O \quad (2)$$

For the SnO_2@m-ZSM-5 nanocomposite, there is a high amount of acidic sites on its framework from the aluminosilicate zeolite (Al-Si-O) support (Figure S11†), which makes more OH^- species easily adsorbed on the surface of SnO_2/m-ZSM-5 as shown in Figure 2D. [48-51] Then the adsorbed OH^- species are proposed to react with SnO_2 nanocrystals as shown in reaction (3).

$$SnO_2 + OH^- + H_2O \leftrightarrow Sn(OH)_x + e^- \quad (3)$$

SnO_2 is a special metal oxide which can readily react with OH^- to form $Sn(OH)_x$, [52, 53] and the $Sn(OH)_x$ species can reversibly release OH^- and recover to SnO_2 as shown in reaction (3), which is similar with the mechanism of NiO,[47,54] Co_3O_4/NiO [55] or $NiCo_2O_4$. [56] So SnO_2 can be a catalyst to accelerate the reaction of (1) and (2), thus the non-precious metal SnO_2/m-ZSM-5 material is believed to be electro-catalytic active in hydrogen oxidation. The cooperative effect between SnO_2 nanocrystals and mesoporous ZSM-5 endows the precious metal-free SnO_2/m-ZSM-5 nanocomposite with similar electrochemical catalytic activity as Pt catalyst, which possesses substantially higher electro-catalytic activity than SnO_2/SBA-15, SnO_2/KIT-6, or SnO_2/ɤ-Al_2O_3 nanocomposites.

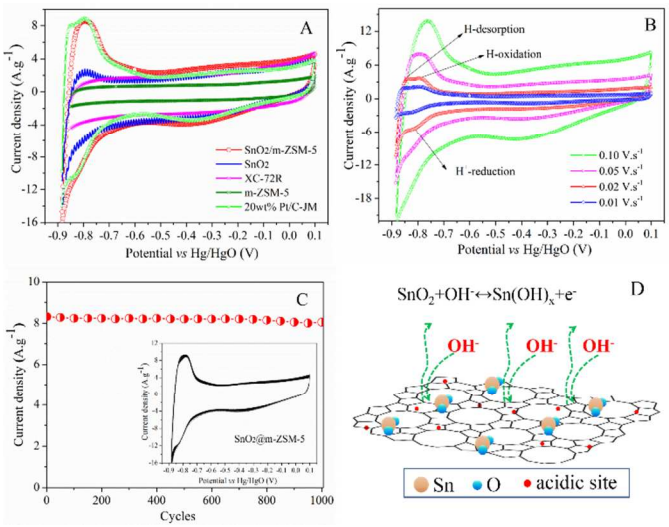

Figure. 2 (A) Current-voltage curves of different samples in 0.5 M NaOH solution at a scan rate of 0.05 V s^{-1} under 20℃; (B) CV curves of as-prepared SnO_2/m-ZSM-5 nanocomposite at varied scan rates; (C) Current *vs* cycling time of prepared SnO_2/m-ZSM-5 at the scan speed of 0.05 V s^{-1} and the cycling CV curves of SnO_2/m-ZSM-5 for 100 times at the same scan speed in the inset; (D) Schematic illustration of the tin hydroxide formation on SnO_2/m-ZSM-5 catalyst in alkaline environment.

Very encouragingly, the SnO_2/m-ZSM-5 nanocomposite shows high catalytic activity for methanol oxidation with a current density of 16 A g^{-1} at the potential of -0.155 V (Figure. 3A), which is close to that of Pt/C in the same 0.8 M methanol electrolyte, though the current peak potential is 25 mV higher than that of the Pt/C (-0.18 V). Methanol oxidation catalytic activity of SnO_2/m-ZSM-5 increases with the increasing methanol concentration. No matter at which concentration, the current density can keep at above 95% of the initial value even after cycled 1000 times (Figure. 3B), indicating the extremely stable catalytic activity of SnO_2/m-ZSM-5 nanocomposite for methanol electro-catalytic oxidation. Moreover, the current density also keeps stable at the constant potential of -0.15 V according to the chronoamperometric results in Figure. 3C, though the current density drops quickly in the first 180 s, further confirming the stable catalytic activity of the prepared SnO_2/m-ZSM-5 material for methanol oxidation. On the contrary, the current density of Pt/C catalyst lowers to 15.51 A g^{-1} after 100 cycles (Figure. S12†), 88.5% of the first cycle (17.52 A g^{-1}) as shown in the inset histogram in Figure. S12†. This may be due to the surface poisoning of Pt catalyst by the intermediate CO_{ads} species during the methanol oxidation. From the CO stripping evolution curves in Figure. 3D, Pt/C catalyst still show a weak CO oxidation peak at the second cycle except for the strong peak (-0.3 V) at the first cycle, while no CO oxidation peak is observed for SnO_2/m-ZSM-5 at the second cycle, though the peak potential of CO oxidation (-0.28 V) is 20mV higher than that of the Pt/C catalyst, suggesting the excellent CO oxidation property of SnO_2/m-ZSM-5. This indicates that the as prepared SnO_2/m-ZSM-5 nanocomposite possesses not only the high catalytic activity for methanol oxidation but also excellent CO tolerance, which can be a satisfactory and applicable precious metal-free anode catalyst in DMFCs.

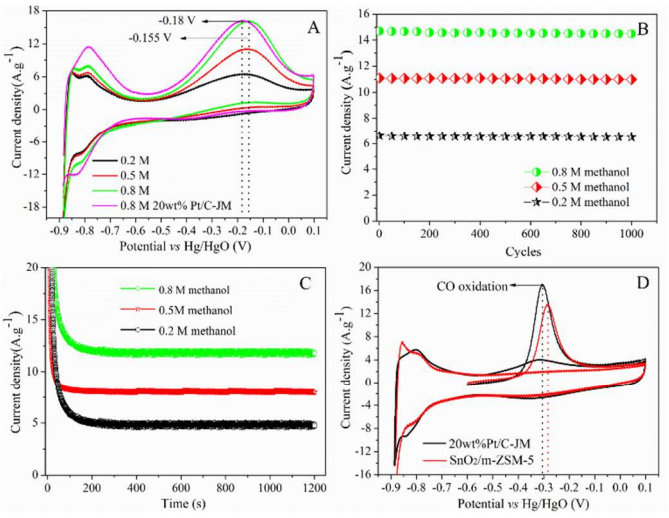

Figure. 3 (A) CV results of prepared SnO_2/m-ZSM-5 nanocomposite for methanol oxidation with different methanol concentrations; (B) Current *vs* cycling time of SnO_2/m-ZSM-5 nanocomposite for methanol oxidation at a constant scan rate of 0.05 V s^{-1}, and (C) Chronoamperometric (current *vs* times) results of methanol oxidation on SnO_2/m-ZSM-5 at constant potential of -0.15 V. (D) CO stripping curves of the samples in 0.5 M NaOH solution at 20℃.

Since the reference samples SnO_2, SnO_2/SBA-15, SnO_2/KIT-6, SnO_2/γ-Al_2O_3 and even SnO_2/ZSM-5 show much lower or even no methanol oxidation activity (see Figure. S13†) in spite of their higher surface areas than that of SnO_2/m-ZSM-5 (see data in Table S1†), catalytic activity of SnO_2/m-ZSM-5 toward methanol oxidation should be attributed to the synergetic catalytic effects between SnO_2 nanocrystals and mesoporous ZSM-5 matrix. First, methanol molecules are adsorbed on the high surface of SnO_2/m-

Energy & Environmental Science Accepted Manuscript

ZSM-5 nanocomposite (shown in Scheme 2A), and then react with the Brønsted acid sites in mesoporous ZSM-5 to form a surface methyl group in reaction (4).[57, 58]

$$CH_3OH \rightarrow -CH_{3ads} + H_2O \quad (4)$$

Secondly, SnO_2 nanocrystals can effectively accelerate the dehydrogenation of $-CH_{3ads}$ species since Sn specie is an effective assistant species during the dehydrogenation of alkane following the reaction (5~7): [59-61]

$$-CH_{3ads} \rightarrow -CH_{2ads} + H^+ + e^- \quad (5)$$

$$-CH_{2ads} \rightarrow -CH_{ads} + 2H^+ + 2e^- \quad (6)$$

$$-CH_{ads} \rightarrow H^+ \text{ (or } -CO_{ads} + H^+) \quad (7)$$

That means, the methyl group ($-CH_{3ads}$) is dehydrogenated in such a stepwise way during the electro-catalytic reaction and consequently the oxidation of methanol is achieved. This is different from the catalytic mechanism of other reported metal oxide anode catalysts such as NiO,[47, 54] Co_3O_4/NiO [55] or $NiCo_2O_4$ [56], which was proposed to react directly with the methanol to form CO_2 during methanol oxidation.

Thirdly, Sn-OH species, efficient to oxidize intermediate CO_{ads} produced during the methanol oxidation, can be formed following the reaction (3) under the assistance of ZSM-5 matrix (Figure 2D) and/or between SnO_2 and water: [62-64]

$$SnO_2 + H_2O \rightarrow Sn\text{-}OH \quad (8)$$

Then, the formed intermediate CO_{ads} species can be promptly oxidized to CO_2 by Sn-OH species following reaction (9), and the CO poisoning phenomenon can be prevented effectively as shown in Scheme 2A.

$$Sn\text{-}OH + CO_{ads} \rightarrow CO_2 + H_2O \quad (9)$$

Thus, methanol molecules can be oxidized continuously following a general reaction (10) on the hierarchically porous SnO_2/m-ZSM-5 nanocomposite.

$$CH_3OH + 8OH^- \rightarrow CO_2/CO_3^{2-} + 6H_2O + 6e^- \quad (10)$$

In addition, the mesoporous pore structure of m-ZSM-5 can shorten the diffusion pathway of reactant molecules and facilitates the transport of products, which also responsible for the accelerated electrochemical reaction of methanol oxidation and consequently the much higher electrochemical catalytic activity of SnO_2/m-ZSM-5 than that of SnO_2/ZSM-5.

Two types of the synergetic effects between SnO_2 nanocrystal and mesoporous ZSM-5 are proposed. The one is that the Brønsted acid sites in mesoporous m-ZSM-5 matrix first adsorb and activate methanol molecules to form surface intermediate−methyl group ($-CH_{3ads}$) species, and then SnO_2 plays as a successional catalyst to make the $-CH_{3ads}$ species dehydrogenated step by step and then thoroughly oxidized (Scheme 2B), following the type II of the synergetic effect "successive catalytic functioning of two components in multistep reactions" proposed by us recently.[65] The other kind of synergetic catalytic effect in our present work is that the Sn-OH species, formed by the reaction between SnO_2 nanoparticle and H_2O, can react with CO_{ads} species produced during the process of methanol oxidation (Scheme 2C), which can effectively prevent the strong adsorption and poisoning of the intermediate CO_{ads} species on the catalyst. Namely, SnO_2 nanoparticle plays a role of mesoporous WO_3 in the anode Pt/WO_3 composite catalyst in DMFC for the prevention of Pt poisoning by CO_{ads}.[66] So this process is typically the type III of the synergetic catalytic effect "degradation prevention of the main catalyst (s) by secondary component(s) for sustained catalytic reactions".[65]

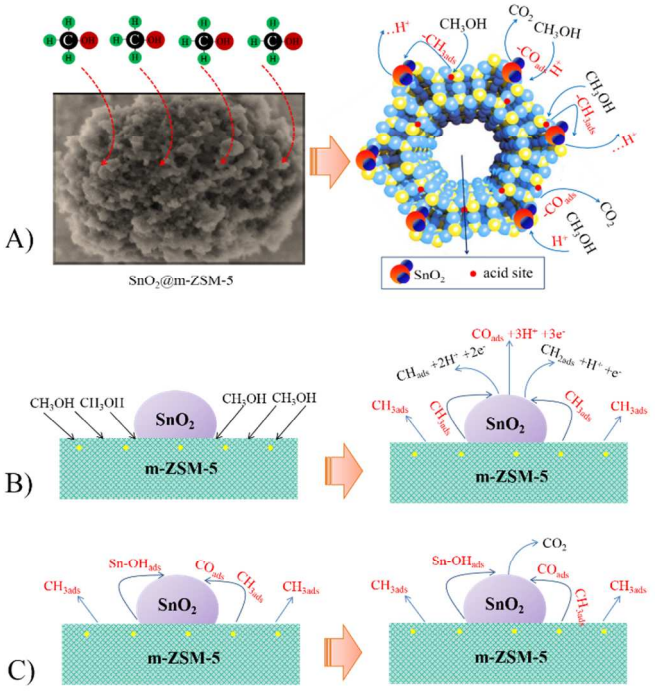

Scheme 2. (A) Schematic illustrations of methanol molecule adsorption on the surface of SnO_2/m-ZSM-5 nanocomposite, and the ball-stick model of methanol oxidation reaction on mesoporous SnO_2/m-ZSM-5 nanocomposite. Schematic illustrations of the proposed synergetic catalytic effects during the methanol oxidation reaction on SnO_2/m-ZSM-5 nanocomposite: (B) Firstly CH_3OH molecules are adsorbed, activated and then react with the Brønsted acid sites in m-ZSM-5 to form surface $-CH_{3ads}$ species, and then dehydrogenized gradually through the catalysis by SnO_2 nanocrystals to achieve the oxidation of methanol; (C) the formed intermediate CO_{ads} species during the methanol oxidation can be promptly oxidized to CO_2 by Sn-OH species resulting from the reaction between SnO_2 nanocrystals and H_2O. Thus, methanol molecules can be oxidized continuously on the hierarchically porous SnO_2/m-ZSM-5 nanocomposite without CO poisoning.

Conclusions

In summary, a novel kind of precious metal-free anode catalyst SnO_2/m-ZSM-5 nanocomposite, with SnO_2 nanocrystals (~3 nm) decorated homogeneously in mesoporous ZSM-5, has been successfully synthesized by hydrothermal and electrostatic interaction approach. The composite catalyst shows comparable electrochemical catalytic activity in methanol oxidation to the commercial 20wt%Pt/C-JM catalyst, and much higher CO tolerance property than the latter in methanol oxidation. The high performance of SnO_2/m-ZSM-5 catalyst is attributed to the synergetic catalytic effects between SnO_2 nanocrystals and mesoporous ZSM-5 material, in which, mesoporous ZSM-5 first adsorb and activate methanol molecules by the frame acidic sites to form methyl group ($-CH_{3ads}$), subsequently, SnO_2 successionally catalyze the dehydrogenation of $-CH_{3ads}$, resulting in final methanol oxidation. In addition, SnO_2 also

Energy & Environmental Science Accepted Manuscript

This journal is © The Royal Society of Chemistry 2012

plays a role of catalyzing the CO_{ads} species into CO_2 by its reaction with Sn-OH in alkaline solution, which is an undesired poisoning intermediate during the methanol oxidation.

Acknowledgements
The authors gratefully acknowledge the financial support from National Key Basic Research Program of China (2013CB933200), National Natural Science Foundation of China (51202278), National Natural Science Foundation of Shanghai (12ZR1435200), state key laboratory of heavy oil processing (SKLOP201402003).

Notes and references

[a] The State Key Laboratory of High Performance Ceramics and Superfine Microstructures, Shanghai Institute of Ceramics, Chinese Academy of Sciences, Shanghai 200050, (P.R. China).
Fax: 86 52413122; Tel: 86 52412712; E-mail: jlshi@mail.sic.ac.cn

† Electronic Supplementary Information (ESI) available: experimental section including materials preparation, characterization, and electrochemical tests. N_2 sorption and pore size distribution curves of reference samples, the characterizations of reference samples including XRD, SEM, TEM, EDX and electrochemical performance test. See DOI: 10.1039/b000000x/.

1 Y. L. Hsin, K. C. Hwang and C. T. Yeh, *J. Am. Chem. Soc*., 2007, **129**, 9999-10010.
2 T. Maiyalagan, *International J. Hydrogen. Energy*., 2009, **34**, 2874-2879.
3 Z. L. Wang, D. Xu, L. M. Wang and X. B. Zhang, *ChemPlusChem*, 2012, **77**, 124-128.
4 Z. Cui, M. Yang and F. J. DiSalvo, *Electrochem. Commun.*, 2013, **33**, 63-67.
5 Z. L. Wang, D. Xu, J. J. Xu and X. B. Zhang, *Chem. Soc. Rev.,* 2014, **43**, 7746-7786.
6 H. Liu, C. Song, L. Zhang, J. Zhang, H. Wang and D. P. Wilkinson, *J. Power Sources*, 2006, **155**, 95-110.
7 S. Pylypenko, A. Borisevich, K. L. More, A. R. Corpuz, T. Holme, A. A. Dameron, T. S. Olson, H. N. Dinh, T. Gennett and R. O'Hayre, *Energy. Environ. Sci.*, 2013, **6**, 2957-2964.
8 J. W. Guo, T. S. Zhao, J. Prabhuram, R. Chen and C.W. Wong, *Electrochim. Acta*., 2005, **51**, 754-763.
9 Z. M. Cui, H. Chen, M. T. Zhao, D. Marshall, Y. C. Yu, H. Abruna and F. J. DiSalve, *J. Am. Chem. Soc*., 2014, **136**, 10206-10209.
10 J. Wang, X. B. Zhang, Z. L. Wang, L. M. Wang, W. Xing and X. Liu, *Nanoscale*, 2012, **4**, 1549-1552.
11 A. M. C. Luna, A. Bonesi, W. E. Triaca, V. Baglio, V. Antonucci and A. S. Arico, *J. Solid State Electrochem.*, 2008, **12**, 643-649.
12 P. Liu, A. Logadottir and J. K. Nørskov, *Electrochim. Acta*., 2003, **48**, 3731-3742.
13 Y. J. Ando, K. Sasaki and R. Adzic, *Electrochem. Commun*., 2009, **11**, 1135-1138.
14 K. G. Nishanth, P. Sridhar, S. Pitchumani, A. K. Shukla, *J. Electrochem. Soc.*, 2011, **158**, B871- B876.
15 C. Koenigsmann and S. S. Wong, *ACS Catal.*, 2013, **3**, 2031-2040.
16 X. Liu, G. Fu, Y. Chen, Y. Tang, P. She and T. Lu, *Chem. Eur. J.*, 2014, **20**, 585-590.
17 J. J. Lv, J. N. Zheng, S. S. Li, L. L. Chen, A. J. Wang and J. J. Feng, *J. Mater. Chem. A*., 2014, **2**, 4384-4390.
18 W. Tokarz, H. Siwek, P. Piela and A. Czerwinski, *Electrochim. Acta*., 2007, **52**, 5565-5573.
19 A. Kowal, M. Li, M. Shao, K. Sasaki, M.B.Vukmirovic, J. Zhang, N. S. Marinkovic, P. Liu, A. I. Frenkel and R. R. Adzic, *Nat. Mater*. 2012, **8**, 325-330.
20 B. Narayanamoorthy, K. R. D. Kasibhatta, M. Eswaramoorthy, and S. S. Balaji, *ACS Catal*., 2014, 4, 3621-3629.
21 J. Wang, X. B. Zhang, Z. L. Wang, L. M. Wang and Y. Zhang, *Energy Environ. Sci.*, 2012, **5**, 6885-6888.
22 Y. Hu, H. Zhang, P. Wu, H. Zhang, B. Zhou and C. Cai, *Phy. Chem. Chem. Phy*., 2011, **13**, 4083-4094.
23 J. N. Zheng, J. J. Lv, S. S. Li, M. W. Xue, A. J. Wang and J. J. Feng, *J. Mater. Chem. A*., 2014, 2, 3445-3451.
24 B. Y. Xia, H. B. Wu, X. Wang and X. W. Lou, *J. Am. Chem. Soc*., 2012, **134**, 13934-13937.
25 J. Rossmeisl, P. Ferrin, G. A. Tritsaris, A. U. Nilekar, S. Koh, S. E. Bae, S. R. Brankovic, P. Strasser and M. Mavrikakis, *Energy. Environ. Sci.*, 2012, 5, 8335-8342.
26 Y. Hu, P. Wu, Y. Yin, H. Zhang and C. Cai, *Appl. Catal. B: Environ*., 2012, *111*, 208-217.
27 Y. Yu, H. L. Xin, R. Hovden, D. Wang, E. D. Rus, J. A. Mundy, D. A. Muller and H. D. Abruna, *Nano letters*, 2012, *12*, 4417-4423.
28 D. A. Stevens, J. M. Rouleau, R. E. Mar, A. Bonakdarpour, R. T. Atanasoski, A. K. Schmoeckel, M. K. Debe and J. R. Dahn, *J. Electrochem. Soc*., 2007, **154**, B566-B576.
29 A. S. Aricò, A. Stassi, C. D'Urso, D.Sebastián and V. Baglio, *Chem. Eur. J.*, 2014, **20**, 10679-10684.
30 P. Strasser, *J. Comb. Chem.*, 2008, **10**, 216-224.
31 M. E. Scofield, C. Koenigsmann, L. Wang, H. Q. Liu and S. S. Wong, *Energy. Environ. Sci.*, 2015, **8**, 350-363.
32 E. Reddington, A. Sapienza, B. Gurau, R. Viswanathan, S. Sarangapani, E. S. Smotkin and T. E. Mallouk, *Science*, 1998, **280**, 1735-1737.
33 W. C. Choi, Y. J. Kim and S. I. Woo, *Catal. Today*, 2002, **74**, 235-240.
34 K. W. Park, J. H. Choi, S. A. Lee, C. Pak, H. Chang and Y. E. Sung, *J. Catal.*, 2004, **224**, 236-242.
35 J. F. Whitacre, T. Valdez and S. R. Narayanan, *J. Electrochem. Soc*., 2005, **152**, A1780-A1789.
36 J. X. Feng, Q. L. Zhang, A. J. Wang, J. Wei, J. R. Chen, J. J. Feng, *Electrochim. Acta*., 2014, **142**, 343-350.
37 M. Choi, K. Na, J. Kim, Y. Sakamoto, O. Teraski and R. Ryoo, *Nature*, 2009, **461**, 246-249.
38 M. Choi, H. S. Cho, R. Srivastava, C. Venkatesan, D. H. Choi and R. Ryoo, *Nat. Mater*., 2006, **5**, 718-723.
39 W. Fan, M. A. Snyder, S. Kumar, P. S. Lee, W. C. Yoo, A. V. McCormick, R. L. Penn, A. Stein and M. Tsapatsis, *Nat. Mater*., 2008, **7**, 984-991.
40 A. Corma, *Chem. Rev*., 1997, **97**, 2373-2420.
41 M. E. Davis, *Nature*, 2002, **417**, 813-821.
42 A. Corma, *J. Catal.*, 2003, **216**, 298-312.
43 X. W. Lou, C. L. Yuan and L. A. Archer, *Adv. Mater*., 2007, **19**, 3328-3332.

Energy & Environmental Science Accepted Manuscript

44 X. W. Lou, C. M. Li and L. A. Archer, *Adv. Mater*., 2009, **21**, 2536-2539.
45 X. W. Lou, J. S. Chen, P. Chen and L. A. Archer, *Chem. Mater*., 2009, **21**, 2868-2874.
46 J. S. Chen, L. A. Archer and X. W. Lou, *J. Mater. Chem.*, 2011, **21**, 9912-9924.
47 Y. Wang, D. D. Zhang, W. Peng, L. Liu and M. G. Li, *Electrochim. Acta*., 2011, **56**, 5754-5758.
48 S. Svelle, C. Tuma, X. Rozanska, T. Kerber and J. Sauer, *J. Am. Chem. Soc*., 2009, **131**, 816-825.
49 I. M. Hill, Y. S. Ng and A. Bhan, *ACS Catal.*, 2012, **2**, 1742-1748.
50 J. Van der Mynsgrugge, J. De Ridder, K. Hemelsoet, M. Waroquier, V. Van Speybroeck, *Chem.Eur. J.*, 2013, **19**, 11568-11576.
51 R. Y. Brogaard, R. Henry, Y. Schuurman, A. J. Medford, P. G. Moses, P. Beato, S. Svelle, J. K. Nørskov and U. Olsbye, *J. Catal*., 2014, **314**, 159-169.
52 H. Yan, L. Ma, G. Chen, S. Wong, W. Man and W. Kwok. *J. Inorganic. Mater*., 1998, **13**, 65-70.
53 X. Wang , S. M. Tabakman , H. Dai , *J. Am. Chem. Soc*., 2008 ,**130** , 8152-.
54 X. L. Tong, Y. Qin, X. Y. Guo, O. Moutanabbir, X. Y. Ao, E. Pippel, L. B. Zhang and M. Knez, *Small*, 2012, **8**, 3390-3395.
55 J. B. Wu, Z. G. Li, X. H. Huang and Y. Lin, *J. Power Sources.*, 2013, **224**, 1-5.
56 M. U. Anu Prathap and R. Srivastava, *Nano Energy*, 2013, **2**, 1046-1053.
57 R. Y. Brogaard, C. M. Wang and F. Studt, *ACS Catal*., 2014, **4**, 4504-4509.
58 A. J. Jones and E. Iglesia, *Angew. Chem. Int. Ed*., 2014, **53**, 1-6.
59 Y. W. Zhang, Y. M. Zhou, A. D. Qiu, Y. Wang, Y. Xu and P. C. Wu, *Catal. Commun*, 2006, **7**, 860-866.
60 S. Furukawa, A. Tamura, K. Ozawa and T. Komatsu, *Appl. Catal. A: Gen*., 2014, **469**, 300-305.
61 J. Wu, Z. M. Peng and A. T. Bell, *J. Catal.*, 2014, **311**, 161-168.
62 T. Frelink, W. Visscher and J. A. R. van Veen, *Electrochem. Acta*., 1994, **39**, 1871-1875.
63 X. M. Wang, J. Lian and Y. Wang, *Int. J. Hydrogen. Energy.*, 2014, **39**, 14288-14295.
64 F. E. Lopez-Suarez, A. Bueno-Lopez, K. I. B. Eguiluz and G. R. Salazar-Banda, *J Power Sources*, 2014, **268**, 225-232.
65 J. Shi, *Chem. Rev*., 2013, **113**, 2139-2181.
66 X. Z. Cui, L. M. Guo, F. M. Cui, Q. J. He, J. L. Shi, *J. Phys. Chem. C.*, 2009, **113**, 4134-4138.

Energy & Environmental Science Accepted Manuscript

This journal is © The Royal Society of Chemistry 2012

As one of the most important clean energy sources, direct methanol fuel cells (DMFCs) have been being an extensive research focus for decades. Unfortunately, relatively fast performance degradation due to the CO poisoning of Pt anode, in addition to the high cost of platinum electrode catalysts, have greatly impeded its commercial development. A novel precious metal-free anode catalyst, mesostructured SnO_2/m-ZSM-5 nanocomposite with SnO_2 nanoparticles (~3 nm) dispersed homogeneously on the out/inner surfaces of matrix has been successfully synthesized, which shows comparable catalytic activity for methanol oxidation to the Pt/C and excellent CO tolerance, resulting from the synergetic effects between mesoporous ZSM-5 matrix and the loaded SnO_2 nanocrystals. Greatly enhanced durability, as compared with Pt/C catalyst, has been achieved due to the CO poisoning-free feature of the as-synthesized SnO_2/m-ZSM-5 (Pt-free) anode catalyst, which is greatly favorable for the future large-scale application of DMFCs not only because of its cost-effectiveness, but also its high electrochemical performance.

Energy & Environmental Science Accepted Manuscript

Table of Contents

The synergetic catalytic effects between mesoporous ZSM-5 matrix and the loaded SnO_2 nanocrystals endow the precious metal-free electrode catalyst SnO_2/m-ZSM-5 nanocomposite high and stable catalytic activity for methanol oxidations.

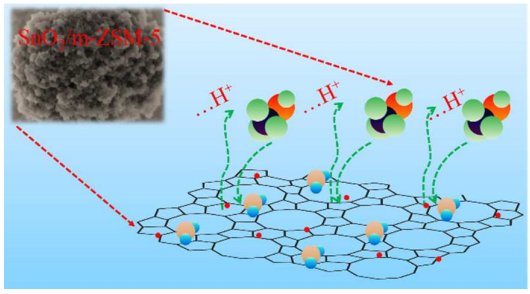

Energy & Environmental Science Accepted Manuscript

Supporting information

SnO_2 Nanocrystals Decorated-Mesoporous ZSM-5 Spheroidicity as Precious Metal-free Electrode Catalyst for Methanol Oxidations

Xiangzhi Cui, Yan Zhu, Zile Hua, Jingwei Feng, Ziwei Liu, Lisong Chen and Jianlin Shi*

The State Key Laboratory of High Performance Ceramics and Superfine Microstructures, Shanghai Institute of Ceramics Chinese Academy of Sciences, Shanghai 200050, (P.R. China).

Experimental

1. Chemicals and Reagents

Aluminium isopropoxide and TEOS (tetraethoxysilane) were obtained from Shanghai J&K, China. Tetrapropylammonium hydroxide (25%) and TPHAC (octadecyldimethyl (3-trimethoxysilyl propyl)ammonium chloride) with 60% methanol were obtained from SIGMA. Zeolite (ZSM-5) with Si/Al=50 was bought form Catalyst Factory of Nankai University.

2. Materials Synthesis

Firstly, ZSM-5 spheroidicity was prepared by hydrothermal method. Typically, 0.3066 g aluminium isopropoxide, 15.624 g TEOS, and 45 g H_2O were added into to Duran bottle under stirring, and then the mixture was stirred continuously for 1 h at room temperature to form an evenly solution. After that, 10.98 g tetrapropylammonium hydroxid, 0.27 g NaOH and 45 g H_2O were added into above

Energy & Environmental Science Accepted Manuscript

solution , and was stirred for 4 h at 40 ℃. Then the temperature was tuned to 100 ℃, and continuously stirred for 48 h. After centrifugation and dried at 100 ℃, the product was obtained. 0.5 g as synthesized material was added into a mixture solution of 100 g H_2O and 60 g ethanol by ultrasonic dispersion, then 30 ml ethanol solution with 0.2 g TPHAC was added drop by drop at 10 ℃ under stirring, and continuously stirred for 5 h. After that, 10 mL (0.03 M) $SnCl_4.5H_2O$ solution was added and continuously stirred for 2h, then 10 ml (1.2 M) NH_3 H_2O solution was dropped slowly under stirring. After centrifugation and dried, the product was calcined at 550 ℃ for 7 h in muffle furnace. Then the SnO_2 nanocrystals decorated homogeneously on ZSM-5 spheroidicity was obtained and named as SnO_2/ZSM-5.

For comparison, zeolite (ZSM-5) with the same Si/Al ratio (Si/Al=50), mesoporous silica, such as SBA-15 and KIT-6, and ɤ-Al_2O_3 were also used as support materials to load SnO_2 nanocrystal by the same method, and the obtained samples were named as SnO_2/ZSM-5, SnO_2/SBA-15, SnO_2/KIT-6, and SnO_2/ɤ-Al_2O_3, respectively. SnO_2 nanopowder was also prepared for comparison, which is synthesized by sol-gel method. Typically, 2.3 g $SnCl_4.5H_2O$ was dissolved in 100 ml H_2O to form a solution of 0.066 M. Then 20 ml (1.2 M) NH_3 H_2O solution was dropped slowly under stirring. After stirred continuously for 5 h at room temperature, the obtained sol was filtered and dried in freezer dryer. The formed gel was grinded in mortar and then calcined at 500 ℃ for 3 h in muffle furnace, then the SnO_2 nanopowder was obtained.

3. Structural Characterizations

Energy & Environmental Science Accepted Manuscript

The powder X-ray diffraction (XRD) patterns of prepared samples were recorded on a Rigaku D/Max-2550V X-ray diffractometer with a Cu-Ka radiation target (40 kV, 40 mA). The N_2 sorption measurements were performed using Micromeritics Tristar 3000 at 77 K, and the specific surface area and the pore size distribution were calculated using the Brunauer–Emmett–Teller (BET) and Barrett–Joyner–Halenda (BJH) methods, respectively. Field emission scanning electron microscopic (FE-SEM) images were performed on a JEOL JSM-6700F field emission scanning electron microscopy. Transmission electron microscopy (TEM) images and Energy-dispersive X-ray spectra (EDX) were obtained on a JEOL 200CX electron microscope operating at 160 kV.

4. Electrochemical measurement

Electrochemical studies of prepared catalyst powders included cyclic voltammetry (CV), CO stripping voltammetry and methanol oxidation current-voltage. Electrochemical measurements were conducted at room temperature in a standard three-electrode configuration that utilized a saturated mercury/mercuric oxide reference electrode (MMO), a Pt mesh counter electrode and a thin-film layer of the catalyst (applied from an ink) as the working electrode. Electrodes were prepared using 1 mg mL^{-1} solutions of catalyst inks made with 10 mg (7 mg catalyst +3 mg carbon black) of the catalyst powder, 7.95 mL of water, 2 mL of 2-propanol (IPA), and 50 μL of 5 wt% Nafion solution. These mixtures w5ere bath sonicated for 20 min and 10 μL of the ink was then applied to the glassy carbon tip. The electrodes were then dried at 40 °C for 30 min. Highly pure N_2 was used prior to the measurements to

Energy & Environmental Science Accepted Manuscript

deaerate the electrolyte. Prior to performing CO stripping voltammetry, the working electrode was electrochemically cleaned in a solution of 0.5 M NaOH by cycling 5 times from -0.885 to 0.10 V. Then, pure CO gas was bubbled into 0.5 M NaOH for 10 min while the working electrode was held at -0.6 V. While the working electrode was still held at -0.6 V, pure N_2 was bubbled for 10 min to purge excess CO from the electrolyte. The potential was then swept to 0.1 V at 20 mV s^{-1} to strip the adsorbed CO from the surface of the working electrode. Two subsequent sweeps from -0.885 to 0.10 V were then performed to ensure that all the bulk CO had indeed been removed from the electrode. For methanol oxidation test, alkaline solution with 0.5 M NaOH and different concentration (0.3, 0.5, 0.8 M) was used as electrolyte, and highly pure N_2 was used prior to the measurements to deaerate the electrolyte.

Energy & Environmental Science Accepted Manuscript

Tables

Table S1. Pore structural parameters of prepared composite catalysts.

Sample	S_{BET}[a]/m^2g^{-1}	D_{BJH}[b]/nm	V_{BJH}[c]/cm^3g^{-1}	SnO_2[d]/%
ZSM-5	394	7.2	0.13	-
m-ZSM-5	402	6.5	0.23	-
SnO_2/ZSM-5	362	6.2	0.1	4.2
SnO_2/m-ZSM-5	371	6.4	0.2	3.8
SnO_2	21	-	-	-
XC-72R	182	-	-	-
SnO_2/SBA-15	730	7.2	1.3	3.9
SnO_2/KIT-6	789	5.9	1.17	3.7
SnO_2/γ-Al_2O_3	180	-	-	4.1

[a] BET surface area, [b] BJH desorption average pore diameter, [c] BJH desorption cumulative pore volume, [d] SnO_2 content (wt %) estimated by EDX spectra.

Energy & Environmental Science Accepted Manuscript

Figures:

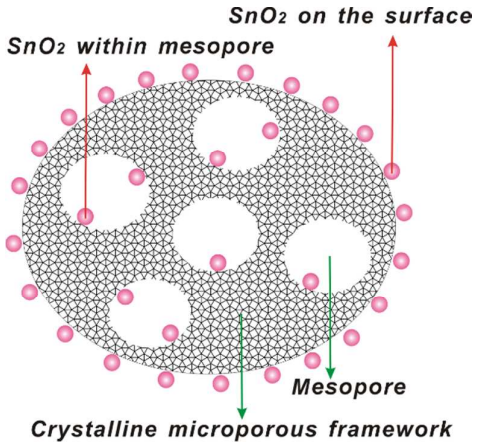

Scheme. S1 Structure schematic of a mesoporous ZSM-5 particle and the distribution of SnO_2 nanoparticles on the out/inner surfaces of it.

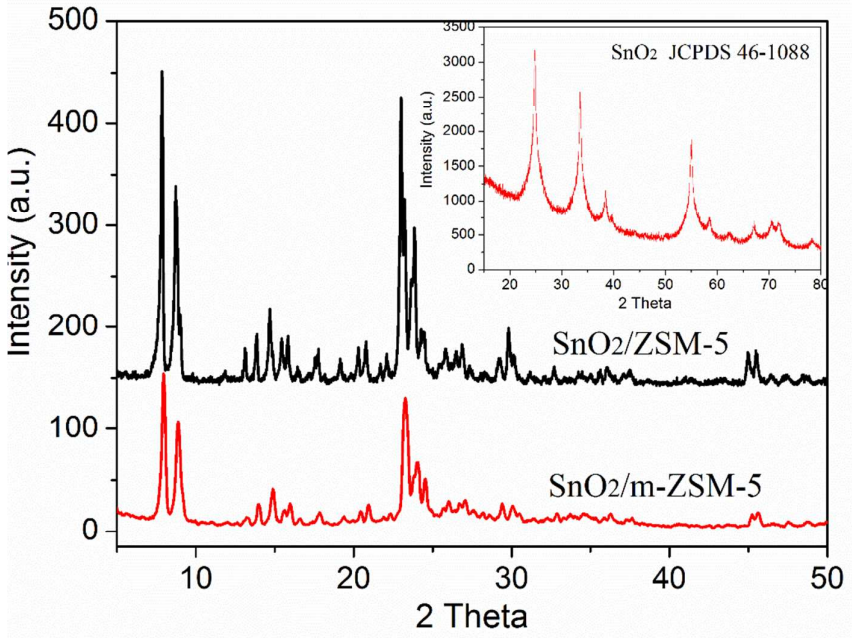

Figure. S1 XRD patterns of the samples SnO_2/m-ZSM-5 and SnO_2/ZSM-5

Energy & Environmental Science Accepted Manuscript

nanocomposites, and the reference sample SnO_2 in the inset.

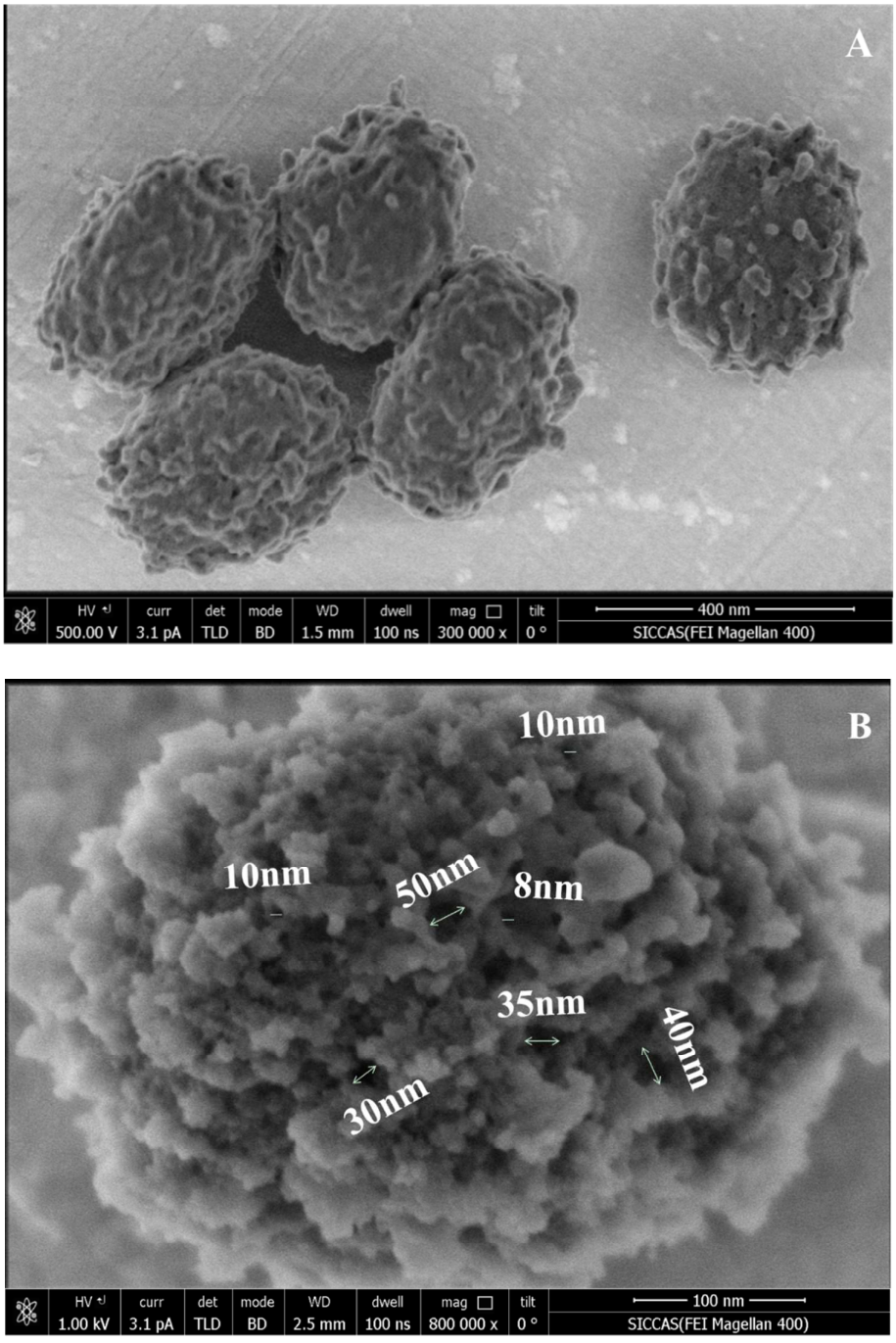

Figure. S2 SEM images with different magnifications of prepared SnO_2/m-ZSM-5 nanocomposite.

Energy & Environmental Science Accepted Manuscript

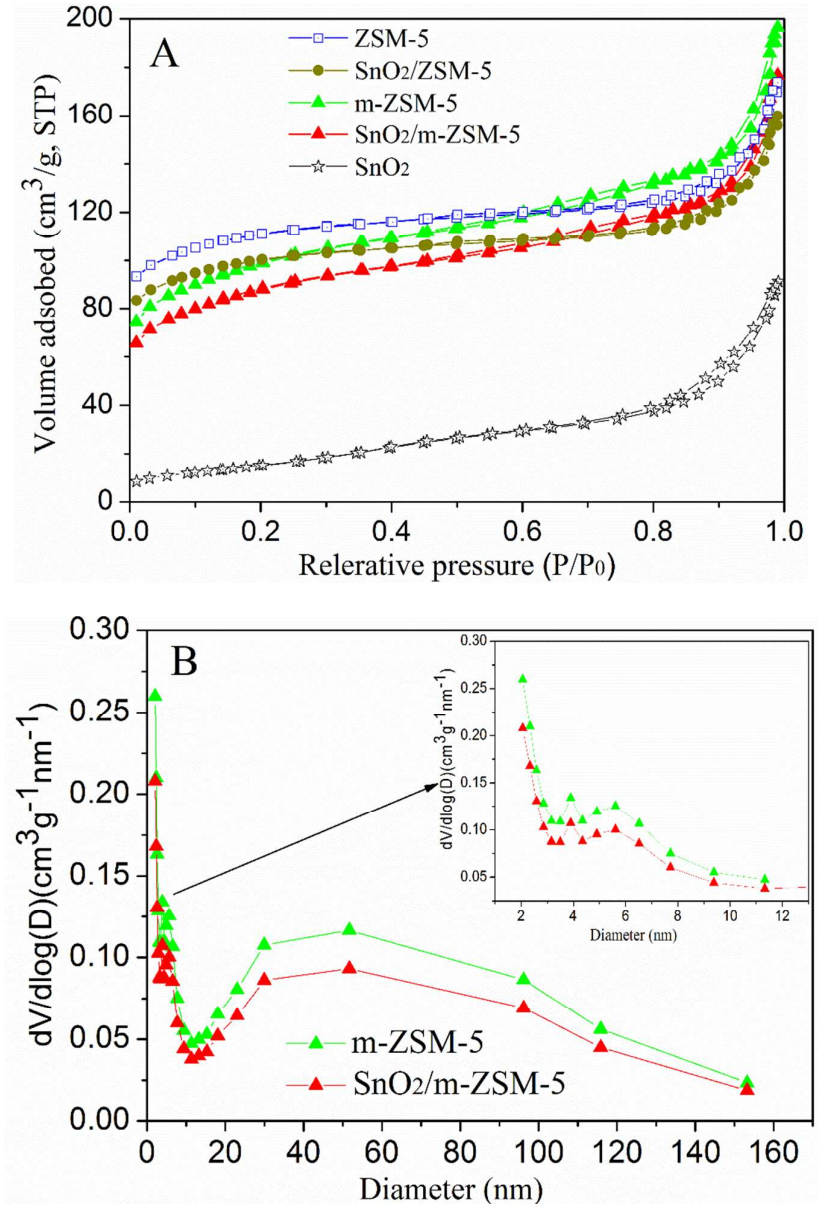

Figure. S3 Nitrogen-sorption isotherms of synthesized samples (A), and the corresponding pore-size distribution curves (B) with the magnified region in the inset.

Energy & Environmental Science Accepted Manuscript

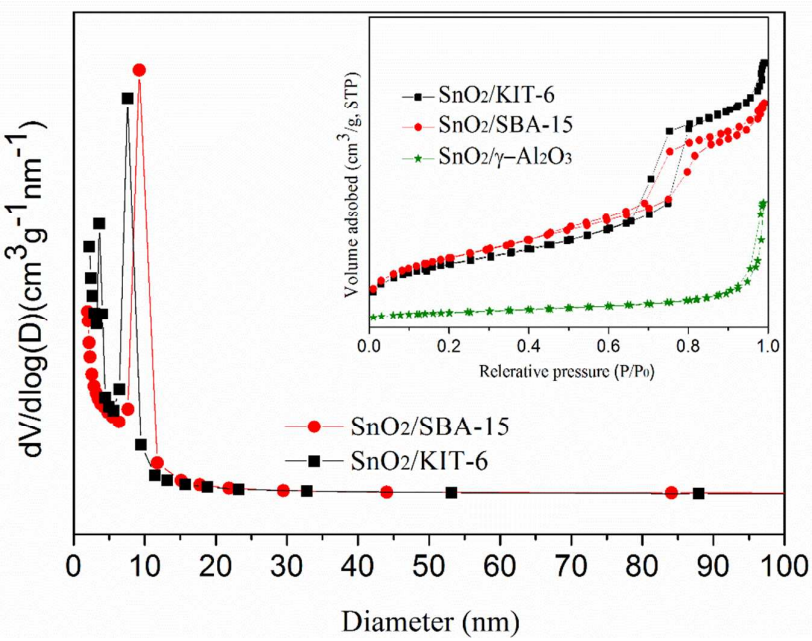

Figure. S4 Nitrogen-sorption isotherms (inset) of reference samples SnO_2/SBA-15, SnO_2/KIT-6 and SnO_2/γ-Al_2O_3, and the corresponding pore-size distribution curves.

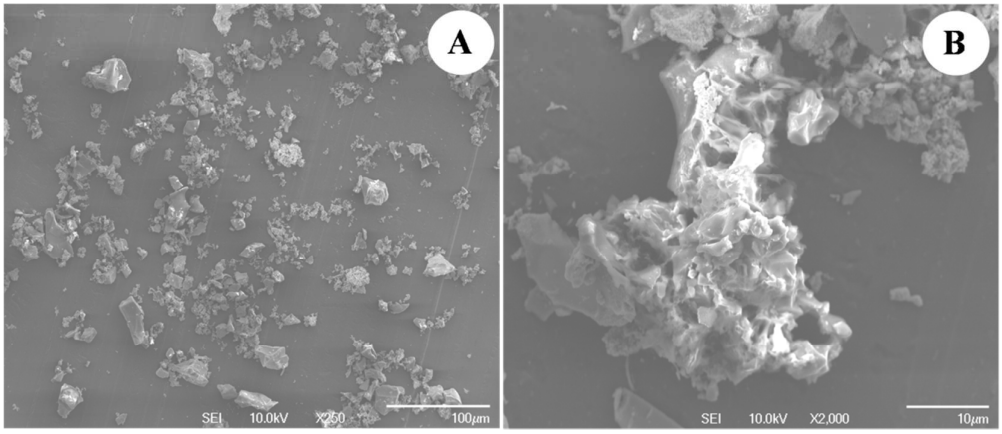

Figure. S5 SEM images of referene sample SnO_2 prepared by sol-gel method.

Energy & Environmental Science Accepted Manuscript

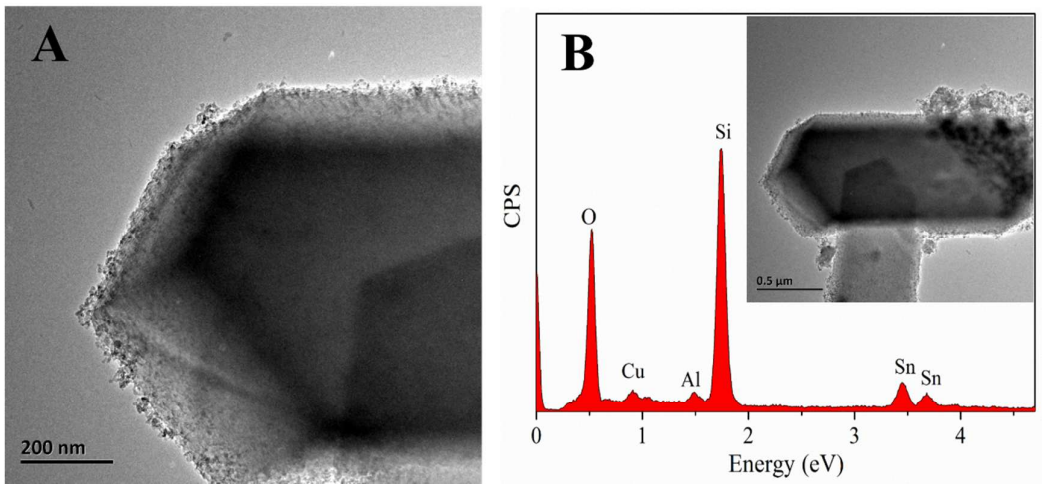

Figure. S6 TEM image of reference sample SnO_2/ZSM-5 (A) and the EDX spectrum (B) of the image in the inset.

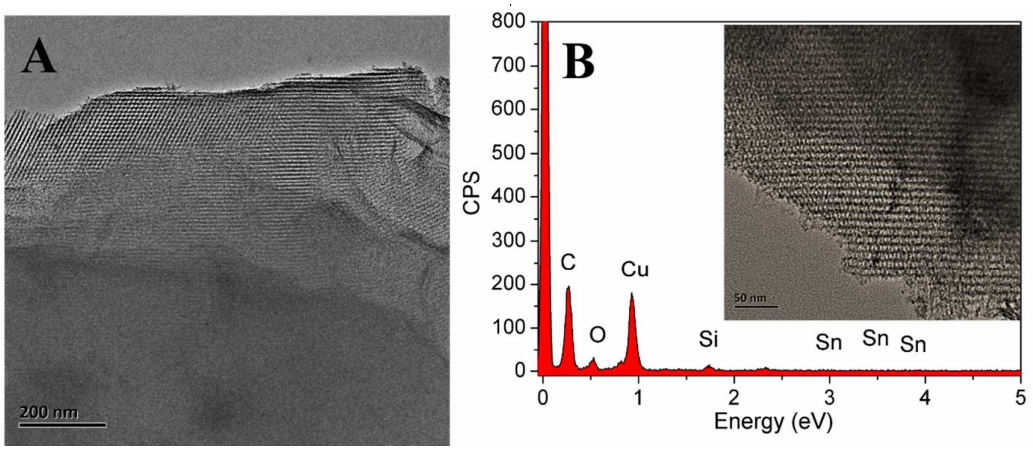

Figure. S7 TEM image of referene sample SnO_2/KIT-6 (A) and the EDX spectrum (B) of the image in the inset.

Energy & Environmental Science Accepted Manuscript

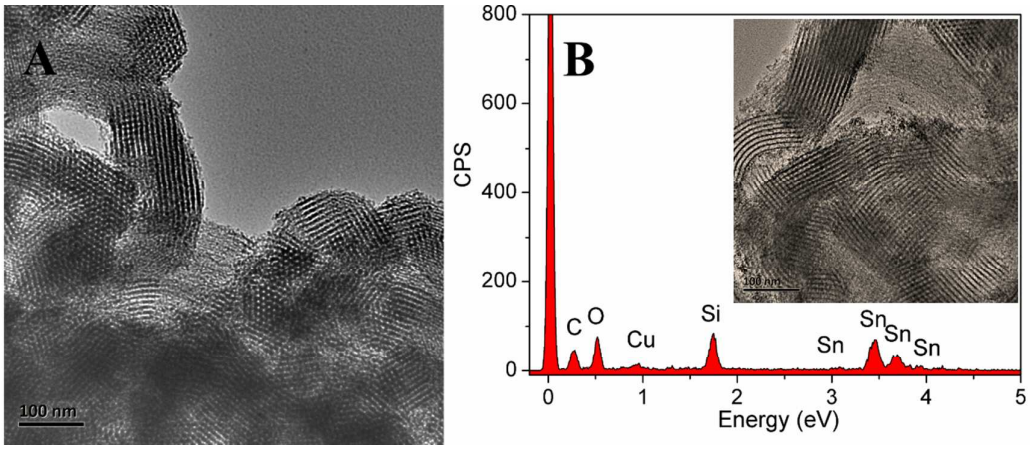

Figure. S8 TEM image of referene sample SnO_2/SBA-15 (A) and the EDX spectrum (B) of the image in the inset.

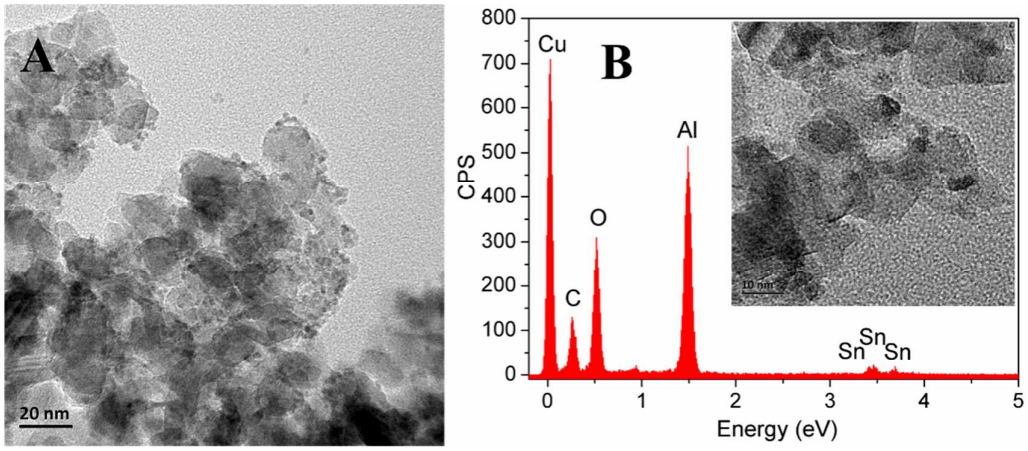

Figure. S9 TEM image of referene sample SnO_2/γ-Al_2O_3 (A) and the EDX spectrum (B) of the image in the inset.

Energy & Environmental Science Accepted Manuscript

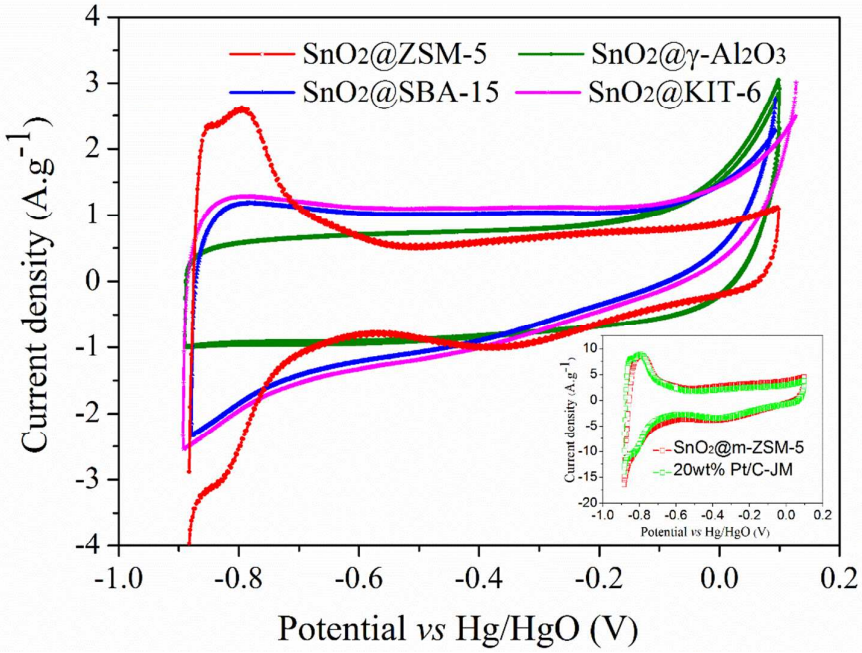

Figure. S10 CV curves of different reference samples in 0.5 M NaOH solution at a scan rate of 0.05 V s^{-1} under 20 ℃, and the CV curves of SnO_2@m-ZSM-5 and commercial 20wt% Pt/C-JM in the inset.

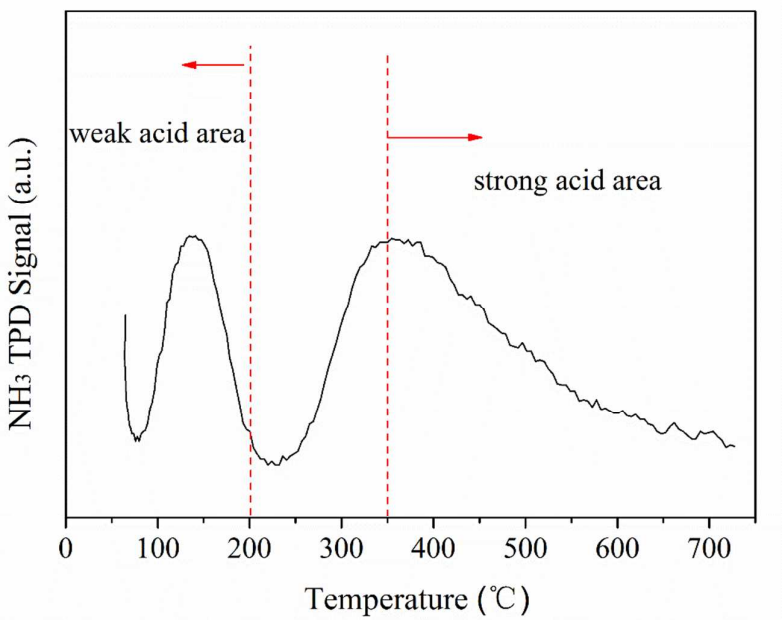

Figure. S11 NH_3-TPD profiles of prepared SnO_2/m-ZSM-5 nanocomposite.

Energy & Environmental Science Accepted Manuscript

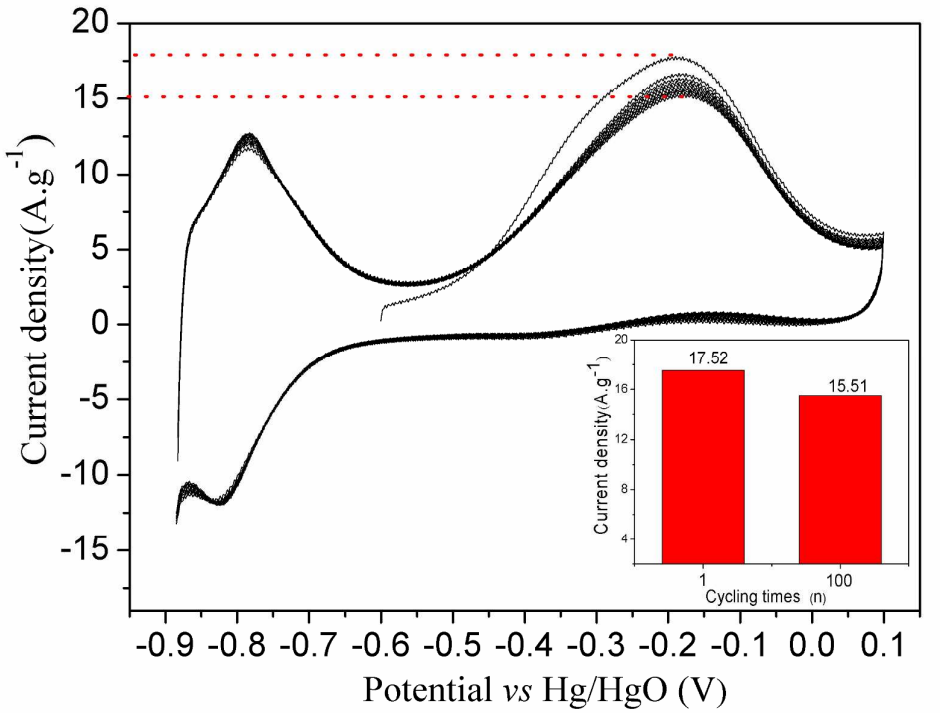

Figure. S12 CV results of methanol oxidation on commercial catalyst 20wt% Pt/C-JM for cycling 100 times in electrolyte solution of 0.5 M NaOH + 0.8 M CH_3OH at a scan rate of 0.05 Vs^{-1} under 20℃, and the current density *vs* cycling time histograms in the inset.

Energy & Environmental Science Accepted Manuscript

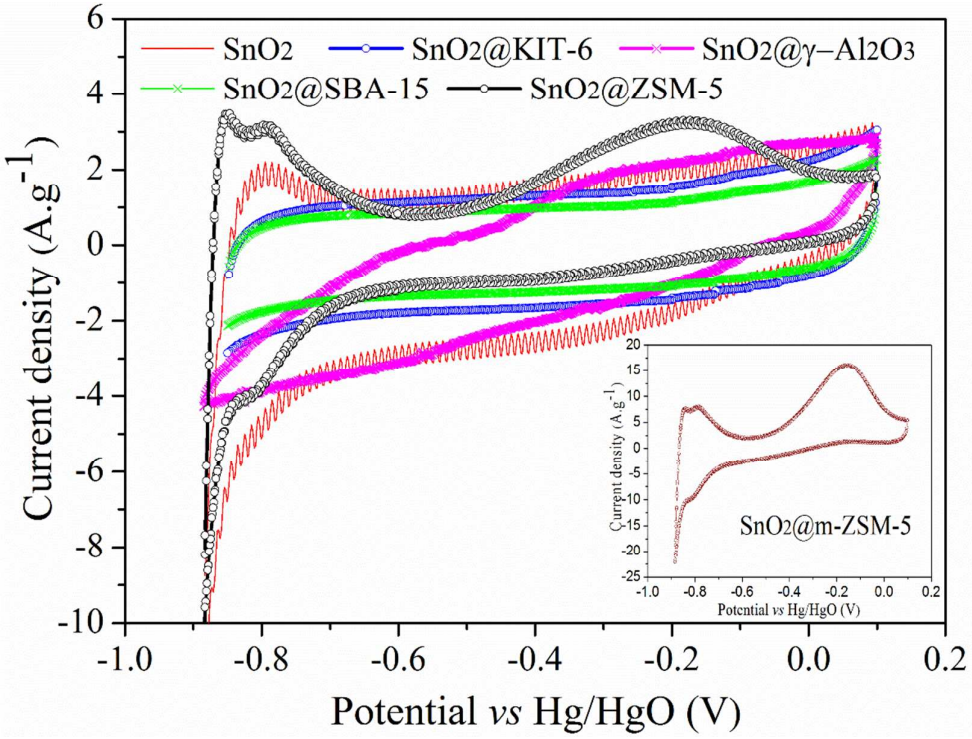

Figure. S13 CV results of samples for methanol oxidation in 0.5 M NaOH + 0.8 M CH_3OH solution at a scan rate of 0.05 Vs^{-1} under 20℃, and the methanol oxidation result of SnO_2@m-ZSM-5 (in the inset) at the same test condition.

Energy & Environmental Science Accepted Manuscript